

# On the thermodynamic stability of PdO surfaces

Jutta Rogal, Karsten Reuter and Matthias Scheffler

*Fritz-Haber-Institut der Max-Planck-Gesellschaft, Faradayweg 4-6, D-14195 Berlin, Germany*

(Dated: Received: 9 October 2003)

As a first step towards understanding the morphology of PdO crystals we performed a systematic full-potential density-functional theory study of all possible  $(1 \times 1)$  terminations of the low-index surfaces of tetragonal PdO. Applying the concept of *first-principles atomistic thermodynamics* we analyze the composition, structure and stability of these PdO orientations in equilibrium with an arbitrary oxygen environment. Within the studied subset of  $(1 \times 1)$  geometries the polar PdO-terminated PdO(100) orientation turns out to be surprisingly stable over the whole range of experimentally accessible gas phase conditions. Setting up a constrained *Wulff construction* within the compiled data set, this PdO(100)-PdO facet correspondingly dominates the obtained polyhedron by far. The real PdO crystallite shape will however likely be affected by surface reconstructions, which are not covered by the present study.

## I. INTRODUCTION

Metal oxides are compounds of widespread technological interest, and one field of application is catalysis, where they can act as the active material or the (often not that passive) support<sup>1,2</sup>. To obtain a microscopic understanding of the function of these compounds in such applications it is necessary to know their surface atomic structure, which is also influenced by temperature and partial pressures in the environment. This can be particularly important for oxygen containing environments, where the stability of different surface terminations of varying stoichiometry may well be anticipated as a function of oxygen in the surrounding gas phase. Considering the technological importance of oxides the scarcity of such atomic-level information even for well-ordered single-crystal surfaces is surprising. The little that is known stems almost exclusively from ultra-high vacuum (UHV) experiments, and is furthermore largely concentrated on some specific oxides like the vanadium oxides, rutile ( $\text{TiO}_2$ ) or corundum ( $\text{Al}_2\text{O}_3$ )<sup>1,2</sup>. For other oxides often not even the low-energy surface orientations are firmly established, and this also applies for the case of palladium oxide (PdO).

Although PdO is renowned for its high activity in the catalytic combustion of methane<sup>3,4,5,6</sup>, and the involvement of oxidic structures in high-pressure CO oxidation reactions at Pd surfaces is now being discussed<sup>7,8</sup>, virtually no information about the electronic and geometric structure of PdO surfaces is presently available, neither from experiment nor from theory. As a first step we therefore investigate the surface structure and composition of all low-index surfaces of tetragonal PdO in equilibrium with an arbitrary oxygen environment using the concept of *first-principles atomistic thermodynamics*<sup>9,10,11,12</sup> based on density-functional theory (DFT) calculations (Section II). Lacking any experimental data on surface reconstructions we first focus on all possible  $(1 \times 1)$  terminations and set up a constrained Wulff construction for this limited set for the whole range

of experimentally accessible gas phase conditions (Section IIIB+C). This provides a first data base against which future models of reconstructed surfaces may be compared, in particular by how much they would have to reduce the surface free energy in order to have corresponding facets contribute significantly to the real PdO crystal shape. In addition, relatively high surface free energies and work functions obtained for  $(1 \times 1)$  terminations might point at likely candidates for surface reconstructions. Interestingly, within the studied subset of  $(1 \times 1)$  geometries, one termination (PdO(100)-PdO) turns out to be much more stable than all others, and correspondingly dominates our constrained Wulff polyhedron by far. And this although it represents a so-called polar termination, which are traditionally dismissed on electrostatic grounds<sup>13,14</sup> (Section IIID).

## II. THEORY

### A. Atomistic thermodynamics

In order to describe the thermodynamic stability of PdO surfaces in an oxygen environment we use DFT total-energy calculations as input to atomistic thermodynamics considerations<sup>9,10,11,12,15,16</sup>, which treat the effect of the surrounding gas phase via the contact with a corresponding reservoir. In equilibrium with such a reservoir the most stable surface structure in the constant temperature and pressure  $(T, p)$ -ensemble minimizes the surface free energy, which is defined as

$$\gamma(T, \{p_i\}) = \frac{1}{A} \left[ G - \sum_i N_i \mu_i(T, p_i) \right] \quad . \quad (1)$$

Here  $G$  is the Gibbs free energy of the solid with the surface of area  $A$ , to which in a supercell calculation with symmetric slabs both the top and bottom surface contribute equally.  $\mu_i(T, p_i)$  is the chemical potential of the various species  $i$  present in the system, i.e. in this case

$i = \text{Pd, O}$ .  $N_i$  gives the number of atoms of the  $i$ th component in the solid. For not too low temperatures and sufficiently large particles bulk PdO may further be assumed as a second thermodynamic reservoir with which the surface is equilibrated. This constrains the chemical potentials of O and Pd to the Gibbs free energy of bulk PdO,  $g_{\text{PdO}}^{\text{bulk}}$  (where the small  $g$  denotes the Gibbs free energy per formula unit), and allows to eliminate  $\mu_{\text{Pd}}$  from eq. (1). The remaining quantities to be determined for the calculation of the surface free energy are then the chemical potential of the oxygen gas phase, as well as the difference in Gibbs free energies of slab and bulk PdO.

The computation of the prior is straight-forward, as  $\mu_{\text{O}}$  is completely fixed by the surrounding gas phase reservoir, which may well be approximated as an ideal gas. Ideal gas laws then relate the chemical potential to temperature and pressure<sup>15,17</sup>, and we will convert the dependence of the surface free energy on  $\mu_{\text{O}}(T, p)$  in all figures also into the more intuitive pressure scales at  $T = 300 \text{ K}$  and  $T = 600 \text{ K}$ . The second input to  $\gamma(T, p)$ , i.e. the Gibbs free energy difference of the bulk phase and the slab, receives contributions from changes in the vibrational and configurational degrees of freedom at the surface, as well as from the  $pV$ -term and as leading contribution from the difference in total energies. From a dimensional analysis, the  $pV$ -term may well be neglected<sup>15</sup>. The configurational contribution for a system like PdO can further be estimated as below  $5 \text{ meV}/\text{\AA}^2$ ,<sup>16</sup> again negligible for a study that aims at a first, rather coarse comparison of different  $(1 \times 1)$  surface terminations.

The vibrational contribution can be obtained from first-principles using the computed phonon density of states (DOS) at the surface and in the bulk, cf. e.g. ref. 18. Alternatively, the Einstein approximation to the phonon DOS can be employed to get an order of magnitude estimate<sup>15</sup>. Allowing a 50% variation of the characteristic frequency<sup>19</sup> of each atom type at the surface, the vibrational contribution to the surface free energy at all considered PdO terminations stays in this model always within a range of about  $10\text{-}20 \text{ meV}/\text{\AA}^2$  for all temperatures up to  $T = 600 \text{ K}$ . Although this is certainly not a small contribution in general anymore, we will nevertheless neglect it in this particular study. Being interested in a coarse, first screening of the stability of various PdO terminations, it will become apparent below that even a  $10\text{-}20 \text{ meV}/\text{\AA}^2$  contribution will not affect the physical conclusions drawn. If in other studies a higher accuracy is required, the vibrational term may either be taken into account by e.g. simplified treatments of the most relevant vibrational modes<sup>20</sup>, or eventually by a full DFT calculation of the phonon DOS. Here, we will neglect it however, and may with all other approximations discussed in this section then replace the difference of bulk and slab Gibbs free energies entering into the computation of  $\gamma(T, p)$  simply by the corresponding difference of total energies.

## B. DFT basis set and convergence

The DFT total energies that are thus needed are obtained using a mixture of the full-potential augmented plane wave + local orbitals (APW+lo) and the linear augmented plane wave (LAPW) method together with the generalized gradient approximation (GGA) for the exchange-correlation functional<sup>21</sup> as implemented in the WIEN2k code<sup>22,23,24</sup>. To simulate the different PdO surfaces we use supercells containing symmetric slabs with 7-11 layers and 12-15  $\text{\AA}$  vacuum between subsequent slabs. The outermost 2-4 layers are fully relaxed for all surfaces. For all orientations we have also performed test calculations with thicker slabs and relaxing more layers, without obtaining any significant changes to the chosen setup ( $\leq 3 \text{ meV}/\text{\AA}^2$  in the surface energy).

The parameters for the mixed APW+lo and LAPW (L/APW+lo) basis set are:  $R_{\text{MT}}^{\text{Pd}} = 1.8 \text{ bohr}$ ,  $R_{\text{MT}}^{\text{O}} = 1.3 \text{ bohr}$ , wave function expansion inside the muffin tins up to  $l_{\text{max}}^{\text{wf}} = 12$ , potential expansion up to  $l_{\text{max}}^{\text{pot}} = 6$ . The Brillouin zone (BZ) integration is performed using Monkhorst-Pack (MP) grids with 6, 8 and 16  $\mathbf{k}$ -points in the irreducible part of the BZ for the (110)/(111), the (100)/(010)/(101)/(011) and the (001) directions, respectively. The energy cutoff for the plane wave representation in the interstitial region is  $E_{\text{max}}^{\text{wf}} = 17 \text{ Ry}$  for the wave function and  $E_{\text{max}}^{\text{pot}} = 196 \text{ Ry}$  for the potential. With these basis sets the surface energies of the different PdO surfaces are converged within  $1\text{-}2 \text{ meV}/\text{\AA}^2$  regarding the  $\mathbf{k}$ -points and  $3\text{-}4 \text{ meV}/\text{\AA}^2$  regarding  $E_{\text{max}}^{\text{wf}}$ . Errors introduced by the fundamental approximation in the DFT approach, i.e. our use of a GGA as exchange-correlation functional, will be commented on below.

## III. RESULTS

Since there is virtually no atomically-resolved information about the structure and composition of crystalline PdO surfaces available from the experimental side, we start our theoretical investigation from a very basic point of view. That is, to get a first idea about the geometric and electronic properties of different PdO surfaces we focus here on a rather coarse comparison of the subset of all possible  $(1 \times 1)$  terminations of the low-index surfaces of tetragonal PdO.

### A. Geometric bulk and surface structure

PdO crystallizes in a tetragonal structure within the space group  $D_{4h}^9$ <sup>25</sup>. There are two formula units of PdO in the tetragonal unit cell with Pd atoms at all corners and in the centre, and O atoms at  $(0, 1/2, 1/4)$ ,  $(0, 1/2, 3/4)$ ,  $(1, 1/2, 1/4)$  and  $(1, 1/2, 3/4)$ , as shown in Fig. 1. All Pd resp. O atoms are equivalent, with each Pd atom planar coordinated by 4 oxygen atoms, and each O atom tetrahedrally surrounded by 4 Pd atoms. Within

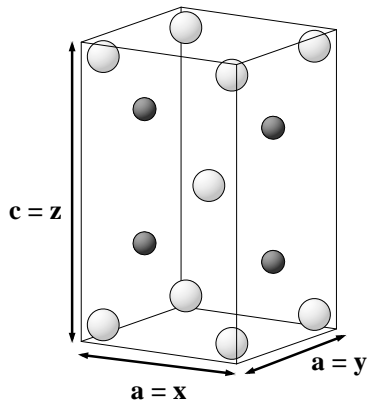


FIG. 1: The tetragonal bulk unit cell of PdO. Small dark spheres indicate oxygen atoms, large light ones Pd atoms.

our DFT-GGA approach the optimized lattice constants of the PdO unit cell are obtained as  $a = 3.051 \text{ \AA}$  and  $c = 5.495 \text{ \AA}$ , which is in reasonably good agreement with the experimental lattice constants,  $a_{\text{exp}} = 3.043 \text{ \AA}$  and  $c_{\text{exp}} = 5.336 \text{ \AA}$ <sup>25</sup>.

Due to the tetragonal structure of the PdO unit cell, there are 5 inequivalent low-index orientations, each with 2-3 different  $(1 \times 1)$  surface terminations. The PdO(100) surface (parallel to the  $yz$ -plane) is equivalent to the (010) surface (parallel to the  $xz$ -plane). For this surface direction there are two different  $(1 \times 1)$  surface terminations, one containing only Pd atoms in the topmost layer (PdO(100)-Pd), and the other Pd as well as O atoms (PdO(100)-PdO). Schematic drawings of these and all following surface geometries are shown as insets in Fig. 2 below. The PdO(001) surface is parallel to the  $xy$ -plane, and there are again two  $(1 \times 1)$  terminations, one with only Pd atoms (PdO(001)-Pd) and one with only O atoms (PdO(001)-O) in the topmost layer.

For the PdO(101) (equivalent to PdO(011)) surface there exist three different terminations. One termination is stoichiometric cutting the stacking of O-Pd<sub>2</sub>-O trilayers along the (101) direction just between consecutive trilayers (PdO(101)). The other two terminate either after the Pd layer (the O-deficient PdO(101)-Pd) or have two O layers at the top (the O-rich PdO(101)-O). The remaining PdO(110) and (111) directions are on the other hand characterized by alternating layers of Pd and O atoms along the surface normal, exhibiting therefore either a completely Pd (PdO(110)-Pd, resp. PdO(111)-Pd) or a completely O (PdO(110)-O, resp. PdO(111)-O) terminated surface.

Looking at these 11 different  $(1 \times 1)$  terminations we notice that only one of them is stoichiometric. The other 10 exhibit either an excess of oxygen or palladium atoms, and belong thus to the class of so-called *polar* surfaces<sup>13,14</sup>, the stability issue of which will be discussed in more detail in Section IIID.

## B. Surface free energies

As mentioned above we want to analyze the stability of these different PdO surfaces when in contact with an oxygen gas phase characterized by a given O chemical potential. This  $\mu_{\text{O}}(T, p)$  can experimentally (and assuming that thermodynamic equilibrium applies) only be varied within certain boundaries. The lower boundary, which will be called the *O-poor limit*, is defined by the decomposition of the oxide into palladium metal and oxygen. A reasonable upper boundary for  $\mu_{\text{O}}$  on the other hand (*O-rich limit*) is given by gas phase conditions that are so oxygen-rich, that O condensation will start on the sample at low enough temperatures. Appropriate and well-defined estimates for these limits are given by<sup>15</sup>

$$\Delta G_f(T = 0\text{K}, p = 0) < \Delta\mu_{\text{O}}(T, p_{\text{O}_2}) < 0 \quad , \quad (2)$$

where the O chemical potential is referenced with respect to the total energy of an oxygen molecule,  $\Delta\mu_{\text{O}} = \mu_{\text{O}} - (1/2)E_{\text{O}_2}^{\text{total}}$ , and  $\Delta G_f(T = 0\text{K}, p = 0)$  is the low temperature limit for the heat of formation of PdO. Within DFT-GGA we compute  $-0.88 \text{ eV}$  for this quantity, which compares well with the experimental value of  $\Delta G_f^{\text{exp}}(T \rightarrow 0\text{K}, p = 1\text{atm}) = -0.97 \text{ eV}$ <sup>26</sup>. To also consider the uncertainty in these theoretically well-defined, but approximate limits for  $\Delta\mu_{\text{O}}$ , we will always plot the dependence of the surface free energies also some tenths of eV outside these boundaries. From this it will become apparent below that the uncertainty in the boundaries does not affect at all our physical conclusions drawn.

We proceed to show all surface free energy plots of the eleven discussed  $(1 \times 1)$  terminations in Fig. 2. Terminations with an O excess (deficiency) show a negative (positive) slope, i.e. they will become the more favorable (unfavorable) the more O-rich the surrounding gas phase is. Comparing the five plots shown in Fig. 2 the very high stability of the PdO(100)-PdO termination is easily recognized. The only other terminations that exhibit comparably low surface energies are the PdO(101), and towards the O-rich limit the PdO(110)-O and PdO(111)-O surfaces. All other considered terminations are rather high in energy, in particular all those that feature Pd atoms in their outermost layer. Looking at the energy scale in the plots we also notice that this stability ordering will not be affected by the afore discussed 10-20 meV/ $\text{\AA}^2$  uncertainty in our surface free energies.

As already indicated above this uncertainty in the surface energies does not yet include the error due to the choice of GGA as exchange-correlation functional. We have therefore calculated the surface free energies of all considered terminations also within the local density approximation (LDA)<sup>27</sup>. To set up the supercells for these LDA calculations we first optimized the lattice constants for PdO bulk, obtaining  $a_{\text{LDA}} = 2.990 \text{ \AA}$  and  $c_{\text{LDA}} = 5.292 \text{ \AA}$ , i.e. values that are as expected slightly smaller than the afore mentioned experimental lattice constants. After a full relaxation of the 2-4 outermost layers, the relative changes in the surface geome-

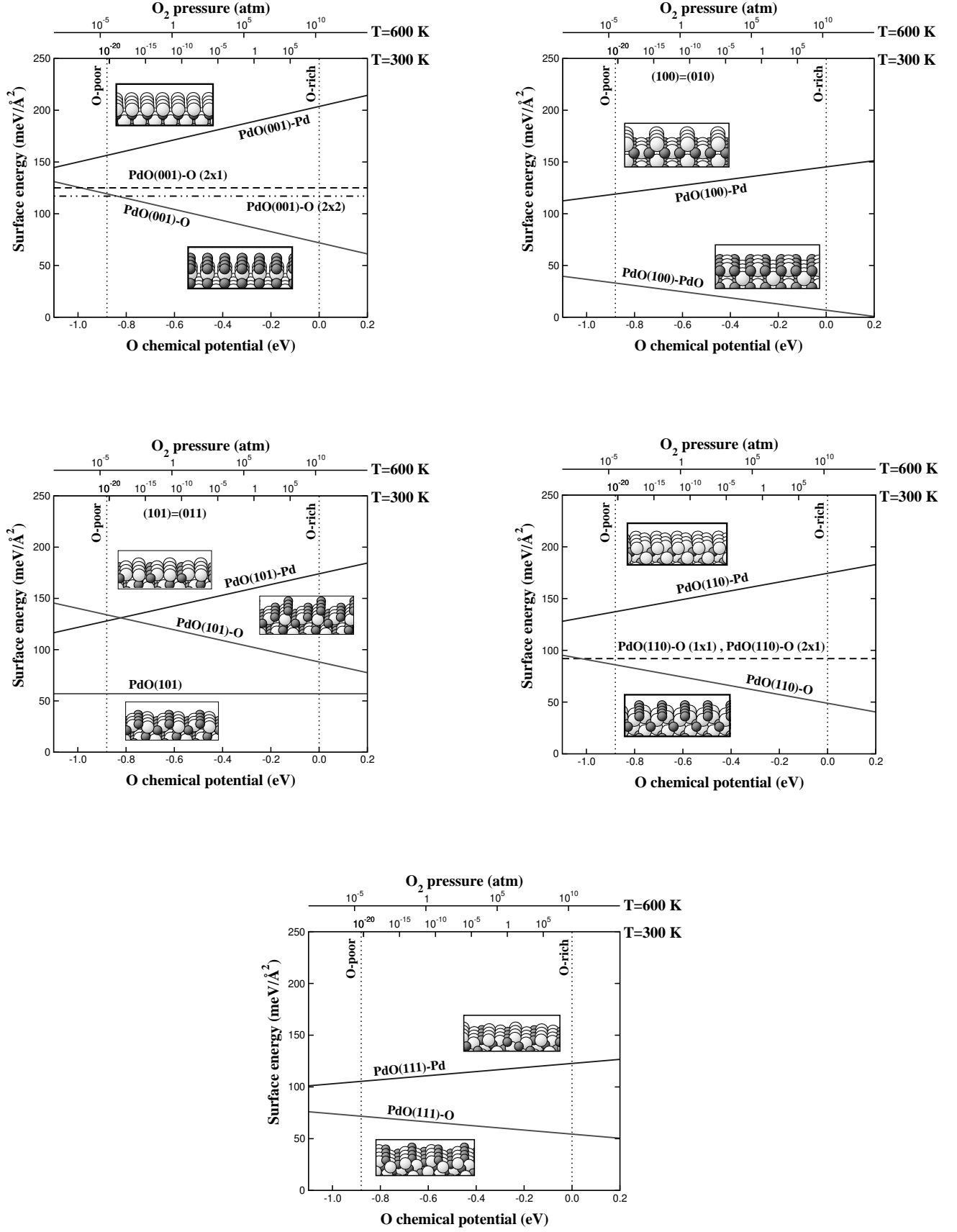


FIG. 2: Surface free energies for the 5 inequivalent low-index PdO surfaces. Solid lines indicate (1 × 1) terminations, and dashed lines larger unit cell reconstructions discussed in Section IIID. The vertical dotted lines specify the range of  $\Delta\mu_O$  considered in this study (see text), while in the top two  $x$  axes the dependence on the O chemical potential has been converted into pressure scales at  $T = 300$  K and  $T = 600$  K. The insets show the surface geometries of the corresponding (1 × 1) terminations (O small dark spheres, Pd large light spheres).

TABLE I: Surface free energies of all low-index PdO ( $1 \times 1$ ) terminations at the oxygen-poor limit, as calculated within the GGA or the LDA. All energies are in  $\text{meV}/\text{\AA}^2$ , and the numbers in brackets denote the energetic difference with respect to the lowest-energy PdO(100)-PdO termination.

Surface termination	$\gamma_{\text{O-poor}}$ GGA		$\gamma_{\text{O-poor}}$ LDA	
PdO(100)-PdO	33	(0)	59	(0)
PdO(100)-Pd	119	(+86)	170	(+111)
PdO(001)-O	119	(+86)	162	(+103)
PdO(001)-Pd	156	(+123)	212	(+153)
PdO(101)	57	(+24)	86	(+27)
PdO(101)-O	134	(+101)	180	(+121)
PdO(101)-Pd	128	(+95)	173	(+114)
PdO(110)-O	86	(+53)	119	(+60)
PdO(110)-Pd	137	(+104)	173	(+114)
PdO(111)-O	72	(+39)	109	(+50)
PdO(111)-Pd	105	(+72)	143	(+84)

tries with respect to these bulk values are found to be very similar to the ones obtained within the GGA. The resulting absolute surface free energies of the eleven terminations in the oxygen-poor limit are listed in Table I (together with the corresponding GGA values). Although the absolute values of the LDA surface energies are  $30\text{-}50\text{ meV}/\text{\AA}^2$  higher than within the GGA, the relative differences between them are within  $10\text{-}30\text{ meV}/\text{\AA}^2$ . This is exemplified in Table I by also indicating the relative energetic difference with respect to the PdO(100)-PdO termination, which is the lowest-energy surface in both the LDA and the GGA. As only this energetic ordering among the considered ( $1 \times 1$ ) terminations enters into the targeted constrained Wulff construction, and we find this ordering to be similar for calculations with two quite different exchange-correlation functionals, we expect the DFT accuracy to be rather high for this system.

### C. Constrained Wulff construction

With the results obtained for the surface free energies of the different ( $1 \times 1$ ) PdO terminations we set up a constrained Wulff construction<sup>28</sup> for a PdO single crystal. Since this construction is constrained to reflect only the studied ( $1 \times 1$ ) terminations, its intention is more to compare the relative energies of different surface orientations, rather than to really predict the equilibrium PdO crystallite shape (which will most likely be affected by surface reconstructions on which we comment below). Since the surface free energies depend on the oxygen chemical potential, the obtained construction will vary with the conditions in the surrounding gas phase. We therefore

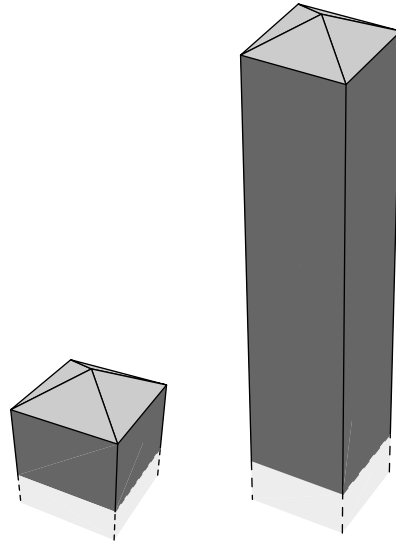


FIG. 3: *Constrained Wulff construction at the oxygen-poor (left) and oxygen-rich limit (right).* The construction is constrained to the studied ( $1 \times 1$ ) terminations and reflects therefore only the relative energies of different PdO orientations, rather than the real PdO crystal shape, which will most likely be affected by surface reconstructions. The polyhedra are symmetric with respect to the  $xy$ -plane, and only the upper half is shown correspondingly.

present in Fig. 3 the Wulff polyhedra for the two considered extremes, i.e. in the O-poor and the O-rich limit. Due to the tetragonal symmetry of PdO, the polyhedra are symmetric with respect to the  $xy$ -plane indicated in Fig. 1, and only the upper half of each polyhedron is shown correspondingly.

As one would already assume from the stability plots in Fig. 2, the low-energy PdO(100)-PdO surface forms the largely dominating facet (rectangular, dark gray facets) at both the O-poor and the O-rich limit of  $\Delta\mu_{\text{O}}$ . The other triangular, light gray facets are built by the stoichiometric PdO(101) surface termination. All other investigated terminations do not contribute at all to the present construction, since the corresponding planes lie outside of the polyhedra and do not cross them at any point. The polyhedra in Fig. 3 are scaled in a way, that the absolute value of the area belonging to the PdO(101) termination is the same in the O-poor and O-rich limit, since the surface free energy of this termination is also constant with respect to  $\Delta\mu_{\text{O}}$ . In turn, the remaining surface area built up by the O-rich PdO(100)-PdO termination increases strongly in going from O-poor to O-rich limit. In the prior limit, this termination forms already 72% of the whole area of the polyhedron, while at the latter limit this fraction has increased to even 94%. As would already be expected from the similar relative energy differences, these Wulff construction properties are also almost equally obtained within the LDA: again the

TABLE II: Minimum energy by which surface reconstructions at the various facets would have to lower the surface free energy, in order for the facets to touch the presently obtained constrained Wulff polyhedron (touching). Additionally, the corresponding lowering required for the facet to cover approximately 10% of the total surface area of the polyhedron is listed (10% area). All energies in  $\text{meV}/\text{\AA}^2$  (and percent changes) are given with respect to the lowest-energy  $(1 \times 1)$  termination of the corresponding orientation.

Orientation	Touching	10% area
Oxygen-poor:		
(001)	-54 (-45%)	-67 (-56%)
(110)	-40 (-47%)	-44 (-51%)
(111)	-7 (-10%)	-16 (-22%)
Oxygen-rich:		
(001)	-7 (-10%)	-42 (-58%)
(110)	-39 (-80%)	-41 (-84%)
(111)	-1 (-2%)	-20 (-37%)

$\text{PdO}(100)\text{-PdO}$  and  $\text{PdO}(101)$  terminations are the only ones contributing to the polyhedron, and the  $\text{PdO}(100)\text{-PdO}$  facet covers 66% (82%) of the surface area in the O-poor (O-rich) limit. Although such a comparison between two functionals forms no formal proof, we would therefore assume the obtained shape to be quite accurate with respect to this DFT approximation.

This does, however, not comprise the major limitation of our study, given by the restriction to  $(1 \times 1)$  terminations. Surface reconstructions could considerably lower the surface free energy of any of the  $\text{PdO}$  surfaces and correspondingly significantly influence the overall shape of the Wulff polyhedron. Unfortunately, to the best of our knowledge no experimental information on such surface reconstructions is presently available for crystalline  $\text{PdO}$ . Without any such information, not even on the surface periodicity, the phase space of possible reconstructions is simply too huge to be assertively screened by today's first-principles techniques alone<sup>29</sup>. Until such information becomes available from experiment, the best we can do at the moment, is to check by how much such surface reconstructions would have to lower the surface free energy in order to give rise to significant changes in the real  $\text{PdO}$  crystal shape compared to the constrained construction presented in this study. This check is done for the three orientations presently not contributing to the exterior of the polyhedron, i.e. the (001), (110) and (111) facets, and since the surface reconstructions are of unknown stoichiometry their effect could be different in the O-poor and in the O-rich limit.

Table II lists the corresponding values for each facet, of how much the surface free energy would have to be lowered by a reconstruction (with respect to the lowest-energy  $(1 \times 1)$  termination presently considered in our constrained Wulff construction), such that the facet just touches the current polyhedron. Additionally given is the

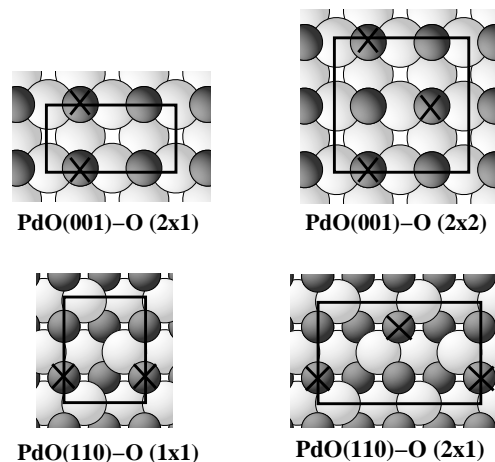


FIG. 4: Unit cells for stoichiometric reconstructions of the  $\text{PdO}(001)\text{-O}$  and  $\text{PdO}(110)\text{-O}$  terminations, achieved by simply removing the oxygen atoms marked with crosses. The two left figures show configurations, where the oxygen atoms are taken out along a row; the right ones, where the oxygen forms a checkerboard pattern.

corresponding value, required to have the reconstruction really contribute significantly to the total Wulff shape, which we consider to be the case when the facet covers approximately 10% of the total surface area. From the compiled data in Table II it seems that rather massive reconstructions would be necessary (both in the O-poor and in the O-rich limit) to have appreciable (001) and (110) facets in the  $\text{PdO}$  equilibrium crystal shape. A much smaller energy reduction would on the other hand be required to have a (111) facet contribute.

#### D. Stability of $\text{PdO}$ surfaces

As already mentioned above only one of the 11 possible  $(1 \times 1)$  terminations, namely the  $\text{PdO}(101)$ , is stoichiometric, whereas all others are so-called polar surfaces, which are not expected to be stable on electrostatic grounds<sup>13,14</sup>. For the three different surface terminations in the (101) direction this ionic model certainly complies with our results, since the stoichiometric  $\text{PdO}(101)$  termination turns out much more stable than the polar  $\text{PdO}(101)\text{-O}$  and  $\text{PdO}(101)\text{-Pd}$  terminations. For the other orientations it is on the other hand not possible at all to truncate the tetragonal  $\text{PdO}$  structure in a  $(1 \times 1)$  cell and achieve charge neutrality; and one might wonder whether this is the reason why e.g. the considered (001) and (110)  $(1 \times 1)$  terminations exhibit such high surface energies? As most obvious guess we therefore performed fully relaxed calculations in larger unit cells, where we simply removed half the O atoms in the top layer in order to achieve stoichiometric terminations. As shown in Fig. 4 there are two possibilities for both the (001) and the (110) orientation to remove these oxygen atoms, either

TABLE III: Work functions for the different  $(1 \times 1)$  PdO surface terminations in eV.

O-terminated	$\Phi$ (eV)	Pd-terminated	$\Phi$ (eV)
PdO(001)-O	7.9	PdO(100)-Pd	4.0
PdO(101)-O	7.7	PdO(001)-Pd	4.8
PdO(110)-O	7.2	PdO(101)-Pd	4.5
PdO(111)-O	5.9	PdO(110)-Pd	4.4
		PdO(111)-Pd	4.7
PdO-terminated	$\Phi$ (eV)	stoichiometric	$\Phi$ (eV)
PdO(100)-PdO	6.4	PdO(101)	5.4

all along a row or in a checkerboard pattern. The corresponding surface free energies are drawn as dashed lines in Fig. 2, and are not at all lower than the corresponding polar  $(1 \times 1)$  O-rich terminations. These results are therefore at variance with the suggestion made by Ciuparu *et al.*, that such a simple removal of O atoms should lead to charge compensated and thus stable PdO(001) and PdO(110) surfaces<sup>5</sup>.

Apparently, charge neutrality is not the dominant feature determining the energetic stability of PdO surfaces, as is also directly reflected in the very low surface free energy of the polar PdO(100)-PdO termination. This points at the most obvious shortcoming of the electrostatic model, namely the assumption that all atoms of one species are identical and in the same charge state, irrespective of whether they are at the surface or in the bulk. As we had shown before<sup>15,30</sup>, structural and electronic relaxation at the surface allows for appreciable deviations from this picture, such that other factors (like an appropriate excess stoichiometry at O-rich conditions) might well overrule the polarity issue.

Still, that there is a different degree of polarity associated with the different terminations, is nicely reflected in the corresponding work functions, cf. Table III. While the work function of the stoichiometric PdO(101) termination is with 5.4 eV in a medium range, the work functions of all Pd-terminated surfaces are about 1.0 - 1.5 eV lower. The ones of the O-terminated surfaces are on the other hand about 1.0 - 2.5 eV higher, just as expected from the ionic model. Even the comparably low work function of the O-terminated PdO(111)-O surface fits into this picture, as there the layer distance to the topmost oxygen atoms is with 0.51 Å significantly smaller than for the other orientations, and leads therefore to a smaller dipole moment.

Discarding the polarity as a major factor governing the surface stability, we proceed to correlate the latter with the binding energy of surface oxygen atoms, as interestingly each most stable  $(1 \times 1)$  termination of each orientation features oxygen atoms in the topmost layer, cf. Fig. 2. The corresponding binding energies with respect to molecular oxygen are shown in Fig. 5, with positive values indicating that O<sub>2</sub> dissociation would be

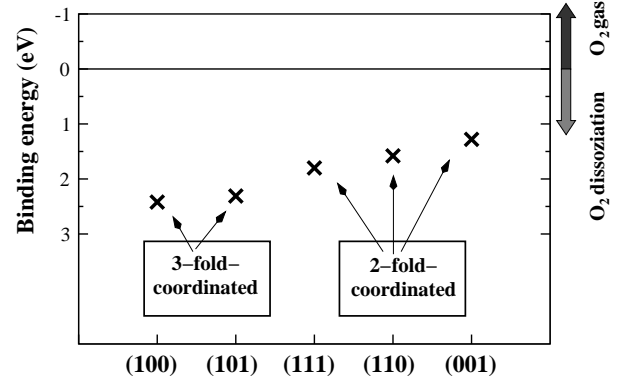


FIG. 5: Binding energies of the topmost oxygen atoms at the most stable  $(1 \times 1)$  termination of the various PdO surfaces. The various orientations are sorted along the  $x$  axes with higher surface free energies to the right. The binding energies are given with respect to a free O<sub>2</sub> molecule.

exothermic. The various orientations are sorted along the  $x$  axes with higher surface energies to the right, revealing a clear correlation. Moreover, there is also a clear correlation with the coordination of the surface atoms: The two most stable terminations, namely the ones contributing to our constrained Wulff polyhedron, feature three-fold coordinated surface O atoms and with  $\sim 2.5$  eV rather strong binding energies. This is followed by the other three orientations, that do not contribute to the present Wulff shape, exhibiting only two-fold coordinated oxygen atoms and somewhat lower binding energies around 1.5 eV. We therefore conclude that the stability of the studied subset of  $(1 \times 1)$  terminations seems primarily governed by the openness of the surface orientation, i.e. whether its geometric structure offers highly-coordinated O binding sites.

#### IV. SUMMARY

In conclusion we have calculated the surface free energies of all low-index  $(1 \times 1)$  PdO terminations in equilibrium with an oxygen environment using the concept of *atomistic thermodynamics*. The PdO(100)-PdO termination exhibits an extraordinarily low surface energy over the entire range of experimentally accessible gas phase conditions. Correspondingly, this facet dominates the Wulff polyhedron constrained to the studied  $(1 \times 1)$  terminations by far, with only the PdO(101) orientation also covering a smaller surface area. The high stability of these two terminations is largely connected to their closed geometric structure, allowing a strong oxygen binding in highly-coordinated surface sites, while the polarity of the non-stoichiometric PdO(100)-PdO termination plays ap-

parently only a minor role. The equilibrium shape of a real PdO crystal is likely to deviate from the presently obtained constrained Wulff polyhedron due to surface reconstructions. Lacking experimental information on such reconstructions, only the minimum energy lowering required to have corresponding facets contribute to the overall crystal shape have been presented.

## V. ACKNOWLEDGEMENTS

Stimulating discussions with M. Todorova are gratefully acknowledged.

- 
- <sup>1</sup> V.E. Henrich and P.A. Cox, *The Surface Science of Metal Oxides*, Cambridge Univ. Press, Cambridge (1994).
  - <sup>2</sup> C. Noguera, *Physics and Chemistry at Oxide Surfaces*, Cambridge Univ. Press, Cambridge (1996).
  - <sup>3</sup> R. Burch and M.J. Hayes, *J. Mol. Catal. A* **100**, 13 (1995).
  - <sup>4</sup> J.G. McCarty, *Catal. Today* **26**, 283 (1995).
  - <sup>5</sup> D. Ciuparu, E. Altman and L. Pfefferle, *J. Catal.* **203**, 64 (2001).
  - <sup>6</sup> D. Ciuparu and L. Pfefferle, *Catal. Today* **77**, 167 (2002).
  - <sup>7</sup> B.L.M. Hendriksen, *Model Catalysts in Action: High-Pressure Scanning Tunneling Microscopy*, Ph.D. thesis, Universiteit Leiden (2003); <http://www.physics.leidenuniv.nl/sections/cm/ip/group/theses.htm#hendriksen>
  - <sup>8</sup> B.L.M. Hendriksen, M.D. Ackermann, and J.W.M. Frenken, (*private communication*).
  - <sup>9</sup> C.M. Weinert and M. Scheffler, In: *Defects in Semiconductors*, H.J. von Bardeleben (Ed.), *Mat. Sci. Forum* **10-12**, 25 (1986).
  - <sup>10</sup> M. Scheffler, In: *Physics of Solid Surfaces – 1987*, J. Koukal (Ed.), Elsevier, Amsterdam (1988). M. Scheffler and J. Dabrowski, *Phil. Mag. A* **58**, 107 (1988).
  - <sup>11</sup> E. Kaxiras, Y. Bar-Yam, J.D. Joannopoulos, and K.C. Pandey, *Phys. Rev. B* **35**, 9625 (1987).
  - <sup>12</sup> G.-X. Qian, R.M. Martin, and D.J. Chadi, *Phys. Rev. B* **38**, 7649 (1988).
  - <sup>13</sup> P.W. Tasker, *J. Phys. C* **12**, 4977 (1979).
  - <sup>14</sup> C. Noguera, *J. Phys.: Condens. Matter* **12**, R367 (2000).
  - <sup>15</sup> K. Reuter and M. Scheffler, *Phys. Rev. B* **65**, 035406 (2002).
  - <sup>16</sup> K. Reuter and M. Scheffler, *Phys. Rev. Lett.* **90**, 046103 (2003); *Phys. Rev. B* **68**, 045407 (2003).
  - <sup>17</sup> D.R. Stull and H. Prophet, *JANAF Thermochemical Tables*, 2nd ed., U.S. National Bureau of Standards, Washington DC (1971).
  - <sup>18</sup> R. Heid, L. Pintschovius, W. Reinhardt, and K.-P. Bohnen, *Phys. Rev. B* **61**, 12059 (2000).
  - <sup>19</sup> J. McBride, K. Hass, and W. Weber, *Phys. Rev. B* **44**, 5016 (1991).
  - <sup>20</sup> Q. Sun, K. Reuter, and M. Scheffler, *Phys. Rev. B* **67**, 205424 (2003).
  - <sup>21</sup> J.P. Perdew, K. Burke, and M. Ernzerhof, *Phys. Rev. Lett.* **77**, 3865 (1996).
  - <sup>22</sup> P. Blaha, K. Schwarz, G.K. Madsen, D. Kvasnicka, and J. Luitz, **WIEN2k**, *An Augmented Plane Wave + Local Orbitals Program for Calculating Crystal Properties*, Karlheinz Schwarz, Techn. Universität Wien, Austria (2001). ISBN 3-9501031-1-2.
  - <sup>23</sup> E. Sjöstedt, L. Nordström, and D.J. Singh, *Solid State Commun.* **114**, 15 (2000).
  - <sup>24</sup> G.K.H. Madsen, P. Blaha, K. Schwarz, E. Sjöstedt, and L. Nordström, *Phys. Rev. B* **64**, 195134 (2001).
  - <sup>25</sup> D. Rogers, R. Shannon, and J. Gillson, *J. Solid State Chem.* **3**, 314 (1971).
  - <sup>26</sup> *CRC Handbook of Chemistry and Physics*, CRC press, Boca Raton FL (1995).
  - <sup>27</sup> J.P. Perdew and Y. Wang, *Phys. Rev. B* **45**, 13244 (1992).
  - <sup>28</sup> G. Wulff, *Z. Kristallogr.* **34**, 449 (1901).
  - <sup>29</sup> E. Lundgren, G. Kresse, C. Klein, M. Borg, J.N. Andersen, M. De Santis, Y. Gauthier, C. Konvicka, M. Schmid, and P. Varga, *Phys. Rev. Lett.* **88**, 246103 (2002).
  - <sup>30</sup> X.-G. Wang, W. Weiss, Sh.K. Shaikhutdinov, M. Ritter, M. Petersen, F. Wagner, R. Schlögl, and M. Scheffler, *Phys. Rev. Lett.* **81**, 1038 (1998).